

## Supporting Information

### Metamaterial-like aerogels for broadband vibration mitigation

Sadeq Malakooti<sup>1, 5, □</sup>, Mohammad I. Hatamleh<sup>1, □</sup>, Rui Zhang<sup>1</sup>, Tahereh Taghvaei<sup>2</sup>,  
Max Miller III<sup>3</sup>, Yao Ren<sup>1</sup>, Ning Xiang<sup>3</sup>, Dong Qian<sup>1</sup>, Chariklia Sotiriou-Leventis<sup>2, §</sup>,  
Nicholas Leventis<sup>2, 4, §</sup>, Hongbing Lu<sup>1, §</sup>

<sup>1</sup>Department of Mechanical Engineering, The University of Texas at Dallas,  
Richardson, TX 75080, U.S.A.

<sup>2</sup>Department of Chemistry, Missouri University of Science and Technology,  
Rolla, MO 65409, U.S.A.

<sup>3</sup>Graduate Program in Architectural Acoustics, Rensselaer Polytechnic Institute,  
Troy, NY 12180, U.S.A.

<sup>4</sup>Current Address: Aspen Aerogels, Inc., 30 Forbes Road, Bldg B,  
Northborough, MA 01532, U.S.A.

<sup>5</sup>Current Address: NASA Glenn Research Center, 21000 Brookpark Rd,  
Cleveland, OH 44135, U.S.A.

□ These authors contributed equally to this work.

§ Corresponding authors: hongbing.lu@utdallas.edu, cslevent@mst.edu, nleventis@aerogel.com

<b>Table of contents</b>	<b>Page #</b>
Figure S1: Test sample configuration for transmissibility measurements.	S-2
Table S1: General material properties of the polyurea aerogels	S-3
Table S2: Pore structure properties of the polyurea aerogels	S-4
Table S3: Basic mechanical and thermal properties of the polyurea aerogels	S-5
Figure S2: (A) The work-flow for the construction of the micromechanical model in order to determine dynamic material properties; (B) Discrete element modeling schematic including particle-particle interactions defined by linear spring stiffness terms and a cut-off radius to truncate the particle-particle interactions; (C) A typical micromechanical model including random packing of 5150 polyurea spherical particles (with average diameter of $2.3 \pm 0.2 \mu\text{m}$ ) and cut-off length of $12 \mu\text{m}$ at bulk density $0.15 \text{ g/cm}^3$ similar to the experimental sample.	S-6
Figure S3: Effective Young's modulus of the micro-computational models at different numbers of particles at similar bulk density and porosity.	S-7
Figure S4: SEM micrograph of the sample with microspheres-with-“hair” (K-index = 1.8) morphology at a lower magnification.	S-8



**Figure S1:** Test sample configuration for transmissibility measurements. The sample is sandwiched between two steel parts and the accelerations are measured using an impedance head at the bottom and an accelerometer at the top of the sample.

**Table S1:** General material properties of the polyurea aerogels

<b>Morphology</b>	<b>Bulk density</b> $(\rho_b, \text{g cm}^{-3})^a$	<b>Skeletal density</b> $(\rho_s, \text{g cm}^{-3})^b$	<b>Porosity</b> $(II, \% \text{ v/v})^c$
Caterpillar-like assemblies of nanoparticles	$0.150 \pm 0.002$	$1.196 \pm 0.004$	$87.5 \pm 0.5$
Random assemblies of nanoparticles	$0.277 \pm 0.002$	$1.201 \pm 0.001$	$76.9 \pm 0.2$
Entangled nanofibers	$0.062 \pm 0.001$	$1.199 \pm 0.015$	$94.8 \pm 1.7$
Microspheres-with-“hair”	$0.151 \pm 0.009$	$1.182 \pm 0.003$	$87.2 \pm 0.8$

<sup>a</sup> Average of 3 samples. <sup>b</sup> Single sample, average of 50 measurements. <sup>c</sup> Porosity (percent of empty space)  $II = 100 \times (\rho_s - \rho_b) / \rho_s$ .

[S-1] Taghvaei, T., Donthula, S., Rewatkar, P. M., Majedi Far, H., Sotiriou-Leventis, C., and Leventis, N., 2019, “*K* -Index: A Descriptor, Predictor, and Correlator of Complex Nanomorphology to Other Material Properties,” ACS Nano, **13**(3), pp. 3677–3690

**Table S2:** Pore structure properties of the polyurea aerogels

<b>Morphology</b>	$V_{\text{Total}}$ ( $\text{cm}^3 \text{g}^{-1}$ ) <sup>a</sup>	<b>Single point volume ads.</b> ( $V_{\text{max}}$ , $\text{cm}^3 \text{g}^{-1}$ ) <sup>b</sup>	<b>BET surface area</b> ( $\sigma$ , $\text{m}^2 \text{g}^{-1}$ )	<b>Average pore diameter</b> ( $f$ , nm) <sup>c</sup>	<b>Particle radius</b> ( $r$ , nm) <sup>d</sup>
Caterpillar-like assemblies of nanoparticles	5.83	0.586	185	126 (13)	14
Random assemblies of nanoparticles	2.78	0.956	151	74 (25)	17
Entangled nanofibers	15.30	0.245	60.2	1020 (16)	42
Microspheres-with-“hair”	5.78	0.080	23.3	1005 (14)	111

<sup>a</sup> Calculated via  $V_{\text{Total}} = (1/\rho_b) - (1/\rho_s)$ . <sup>b</sup> The maximum volume of  $\text{N}_2$  absorbed along the isotherm as  $P/P_0$  approaches to 1.0. <sup>c</sup> Cumulative volume of pores between 1.7 nm and 300 nm from  $\text{N}_2$ -sorption data and the BJH desorption method. <sup>d</sup> By the  $4V/\sigma$  method; for the first number,  $V$  was taken equal to  $V_{\text{Total}} = (1/\rho_b) - (1/\rho_s)$ ; for the number in [brackets],  $V$  was set equal to the maximum volume of  $\text{N}_2$  absorbed along the isotherm as  $P/P_0$  approaches to 1.0. <sup>d</sup> Particle radius,  $r = 3/(\rho_s \times \sigma)$ .

[S-1] Taghvaei, T., Donthula, S., Rewatkar, P. M., Majedi Far, H., Sotiriou-Leventis, C., and Leventis, N., 2019, “ $K$  -Index: A Descriptor, Predictor, and Correlator of Complex Nanomorphology to Other Material Properties,” *ACS Nano*, **13**(3), pp. 3677–3690

**Table S3:** Basic mechanical and thermal properties of the polyurea aerogels

<b>Morphology</b>	<b>Young's modulus (<i>E</i>, MPa)</b>	<b>Ultimate Compressive Strength (<i>UCS</i>, MPa)</b>	<b>Specific energy absorption (<i>U<sub>T</sub></i>, J g<sup>-1</sup>)</b>	<b>Thermal conductivity (mW m<sup>-1</sup> K<sup>-1</sup>)</b>
Caterpillar-like assemblies of nanoparticles	36 ± 1	49 ± 4	23 ± 6	34.0 ± 0.1
Random assemblies of nanoparticles	82 ± 3	157 ± 1	52 ± 1	36.5 ± 0.1
Entangled nanofibers	2.1 ± 0.1	235 ± 1	135 ± 1	31.0 ± 0.1
Microspheres-with-“hair”	6.3 ± 0.4	240 ± 12	65 ± 1	38.7 ± 0.1

[S-1] Taghvaei, T., Donthula, S., Rewatkar, P. M., Majedi Far, H., Sotiriou-Leventis, C., and Leventis, N., 2019, “*K* -Index: A Descriptor, Predictor, and Correlator of Complex Nanomorphology to Other Material Properties,” ACS Nano, **13**(3), pp. 3677–3690

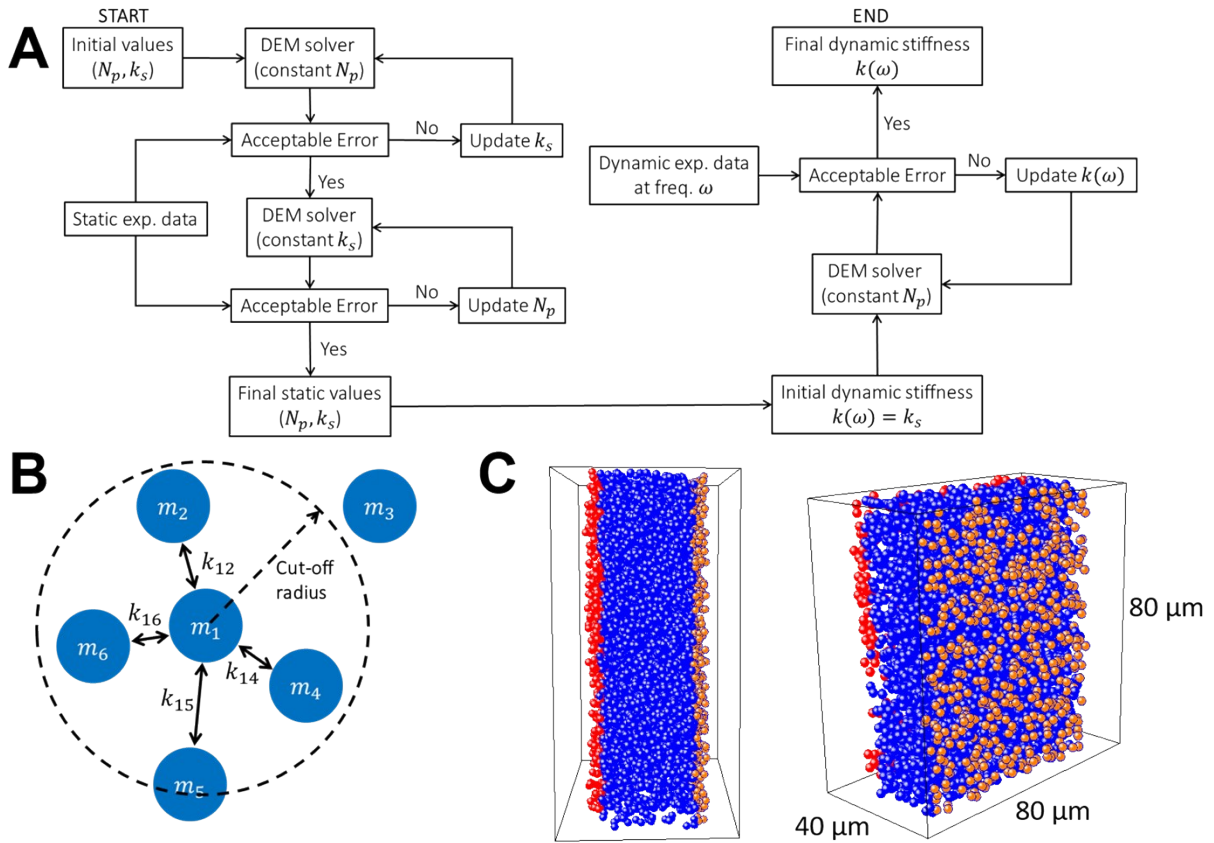


**Figure S2:** (A) The work-flow for the construction of the micromechanical model in order to determine dynamic material properties; (B) Discrete element modeling schematic including particle-particle interactions defined by linear spring stiffness terms and a cut-off radius to truncate the particle-particle interactions; (C) A typical micromechanical model including random packing of 5150 polyurea spherical particles (with average diameter of  $2.3 \pm 0.2 \mu\text{m}$ ) and cut-off length of  $12 \mu\text{m}$  at bulk density  $0.15 \text{ g/cm}^3$  similar to the experimental sample.

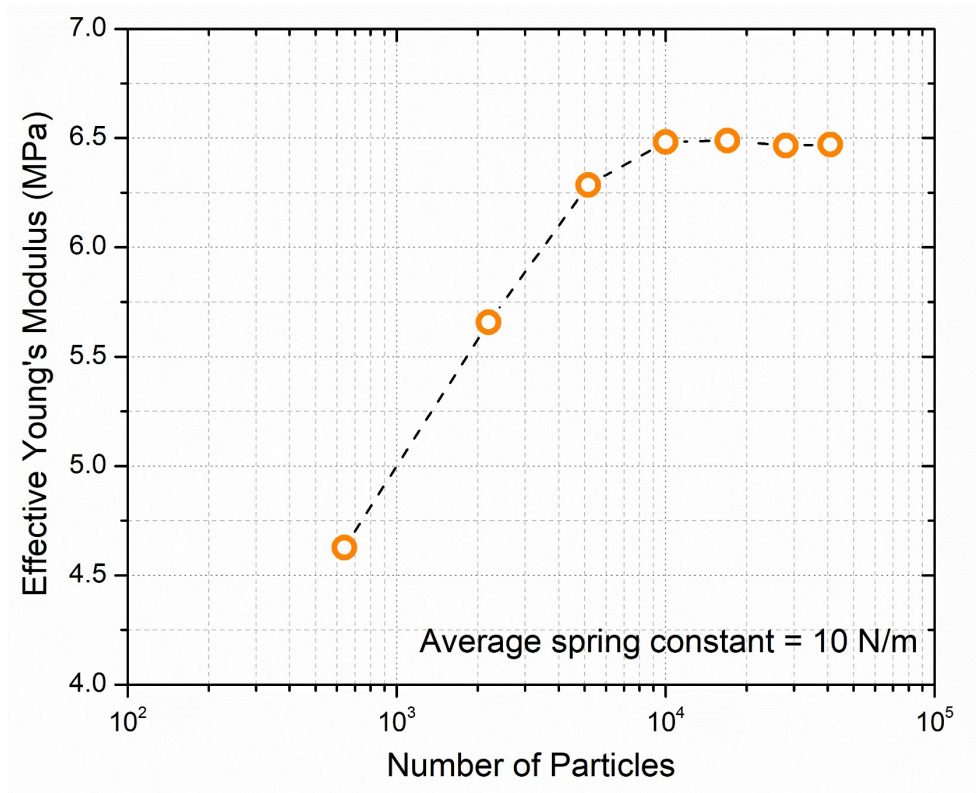


**Figure S3:** Effective Young's modulus of the micro-computational models at different numbers of particles at similar bulk density and porosity.

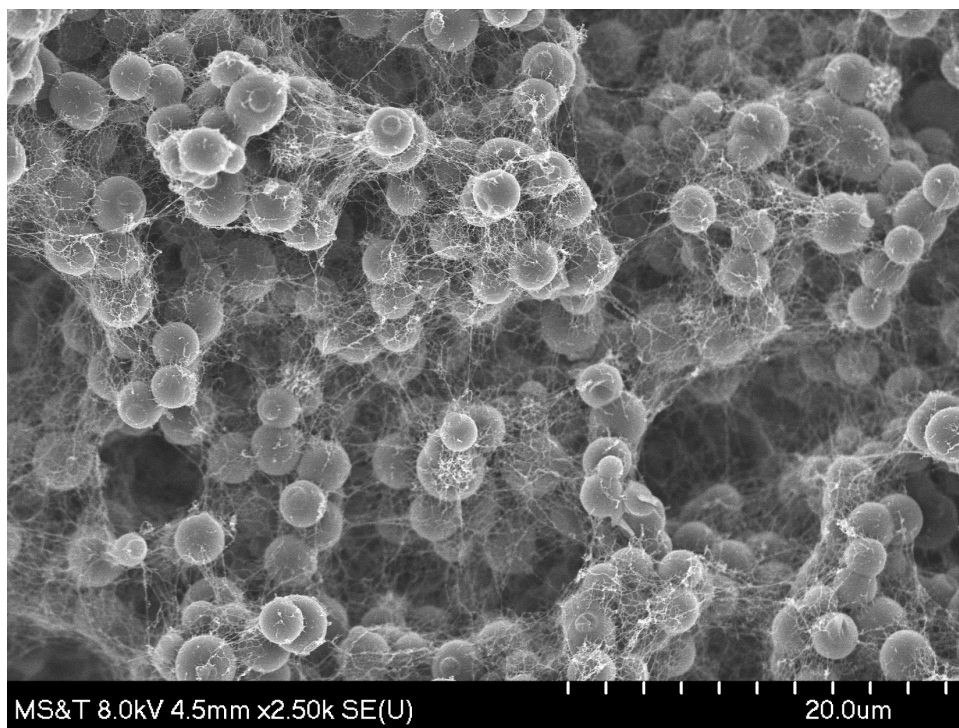


**Figure S4:** SEM micrograph of the sample with microspheres-with-“hair” ( $K$ -index = 1.8) morphology at a lower magnification.